12-2008

# A Reconfigurable Motor for Experimental Emulation of Stator Winding Inter-Turn and Broken Bar Faults in Polyphase Induction Machines (Journal article)

Chia-Chou Yeh

Gennadi Y. Sizov
*Rockwell Automation*

Ahmed Sayed-Ahmed
*Rockwell Automation*

Nabeel Demerdash
*Marquette University*, nabeel.demerdash@marquette.edu

Richard J. Povinelli
*Marquette University*, richard.povinelli@marquette.edu

*See next page for additional authors*

*IEEE Transactions on Energy Conversion*, Vol. 23, No. 4 (December 2008): 1005-1014. DOI. 

# A Reconfigurable Motor for Experimental Emulation of Stator Winding Interturn and Broken Bar Faults in Polyphase Induction Machines

Chia-Chou Yeh
Department of Electrical and Computer Engineering, Marquette University, Milwaukee, WI
Powertrain Advanced Technology Center, General Motors Corporation, Torrance, CA
Gennadi Y. Sizov
Department of Electrical and Computer Engineering, Marquette University, Milwaukee, WI
Ahmed Sayed-Ahmed
Department of Electrical and Computer Engineering, Marquette University, Milwaukee, WI
Nabeel A. O. Demerdash
Department of Electrical and Computer Engineering, Marquette University, Milwaukee, WI
Richard J. Povinelli

Department of Electrical and Computer Engineering, Marquette University, Milwaukee, WI
Edwin E. Yaz
Department of Electrical and Computer Engineering, Marquette University, Milwaukee, WI
Dan M. Ionel
Corporate Technology Center, A. O. Smith Corporation, Milwaukee, WI

## Abstract:

The benefits and drawbacks of a 5-hp reconfigurable induction motor, which was designed for experimental emulation of stator winding interturn and broken rotor bar faults, are presented in this paper. It was perceived that this motor had the potential of quick and easy reconfiguration to produce the desired stator and rotor faults in a variety of different fault combinations. Hence, this motor was anticipated to make a useful test bed for evaluation of the efficacy of existing and new motor fault diagnostics techniques and not the study of insulation failure mechanisms. Accordingly, it was anticipated that this reconfigurable motor would eliminate the need to permanently destroy machine components such as stator windings or rotor bars when acquiring data from a faulty machine for fault diagnostic purposes. Experimental results under healthy and various faulty conditions are presented in this paper, including issues associated with rotor bar-end ring contact resistances that showed the drawbacks of this motor in so far as emulation of rotor bar breakages. However, emulation of stator-turn fault scenarios was successfully accomplished.

## SECTION I. Introduction

Polyphase induction motors have been the workhorse (main prime movers) for industrial and manufacturing processes as well as some propulsion applications. They are commonly used in ac adjustable speed drives where torque and speed control is indispensable. The ruggedness, ease of control, and cost-effective design of squirrel-cage induction motors are the main appealing features to consumers and engineers for the various aforementioned applications. Due to its popularity, there have been many investigations on condition monitoring and fault diagnostics in electric machines throughout the literature, especially squirrel-cage induction motors [1]–[2][3][4][5][6][7][8][9][10][11][12][13][14]. This is because failure of such motors as prime movers can lead to significant undesirable repercussions such as production downtime, financial loss, adverse environmental effects, and possible personnel injury. Consequently, considerable interest in machine fault diagnostics received from industry and academia has prompted researchers to develop excellent state-of-the-art diagnostic techniques for various possible types of faults such as indicated in Fig. 1. The probability of occurrence of such faults is given in Table I (see [15] and [16]). Therein, both the stator and rotor faults account for around 40% of all faults. Accordingly, the main thrust of this paper centers on electrical stator and rotor faults.

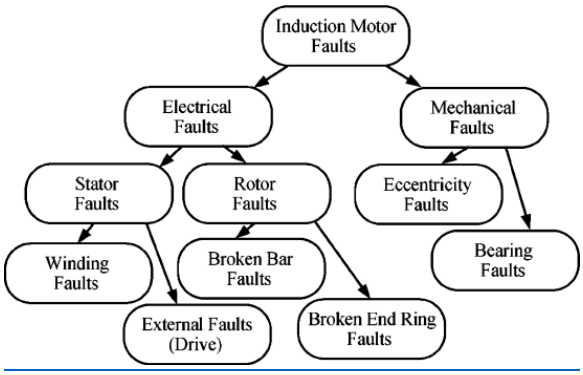

**Fig. 1.** Induction motor fault categories.

**Table I** Percentage of Failures by Major Motor Components

| Major Components | IEEE-IAS [15] % of Failures | IPRI [16] % of Failures |
|---|---|---|
| Bearing Related | 44 | 41 |
| Winding Related | 26 | 36 |
| Rotor Related | 8 | 9 |
| Other | 22 | 14 |

In order to develop improved or novel stator and rotor fault diagnostic methods, extensive research has been done on the dynamic modeling of motor faults. This includes using the time-stepping coupled finite-element state–space technique to incorporate the stator and rotor faults for performance study and analysis [17]. It is desired to compare and verify these motor performances with physical data acquired from an actual motor with selected faults. Comparison between modeled and actual faults can significantly improve the fidelity of the simulation models and lead to improvements in future machine models representing various faulty conditions. Present methods of obtaining motor fault data are time-consuming and often require permanent deformation or destruction of motor components in order to perform the experiments. These actions of destruction of motor components are often irreversible, and hence, require several spare motors or their associated components in order to perform experiments of various fault scenarios. The machine components used for these tests are experiment specific and often require a significant amount of storage space. It was thought that these costly obstacles could be overcome through the use of a reconfigurable induction motor that can physically and experimentally emulate such faults in a reversible manner that avoids permanent damage to motor parts. The main objective of this paper was to develop a reconfigurable induction machine that can be utilized for stator and rotor fault emulation. In the case of stator interturn faults, the circulating current was controlled by varying the resistance between the turns. Whereas, in the case of rotor broken bar faults, these faults were emulated by means of removal of bars from the reconfigurable cage. Accordingly, this paper was not intended for the study of the process of insulation failure in the turns or dielectric/insulation variability around a developing short. In other words, this paper was not intended to characterize the mechanisms behind stator winding insulation breakdowns/failures or rotor bar breakages.

The reconfigurable induction motor, which is the subject of this paper, is a 230/460-V, 60-Hz, six-pole, 5-hp, squirrel-cage three-phase machine. This machine was built with a reconfigurable rotor and also tested with a production-type aluminum die-cast squirrel-cage rotor. It was thought that it may possess the advantages of quick and easy reconfiguration of the motor to produce the desired stator or rotor fault, or a combination of both. In addition, the utilization of the reconfigurable motor eliminates the need to permanently destroy machine components such as stator phase windings or rotor squirrel-cage bars. The thinking behind this effort was that, having the versatility of the reconfigurable motor, large amounts of data can be acquired efficiently for analysis under a variety of different fault configurations or combinations. In this present phase of the paper, the extent of the faults has been limited to stator winding interturn and broken bar faults due to their encompassing of around 40% of all motor faults (see Table I). Issues associated with the reconfigurable rotor cage design and resulting experimental data are fully detailed in this paper. The cast-type squirrel-cage was used to establish a healthy motor performance database of current and voltage waveforms, as well as fast Fourier transform (FFT) spectra [4], [5] and pendulous oscillation swing angle profiles [7]–[8][9].

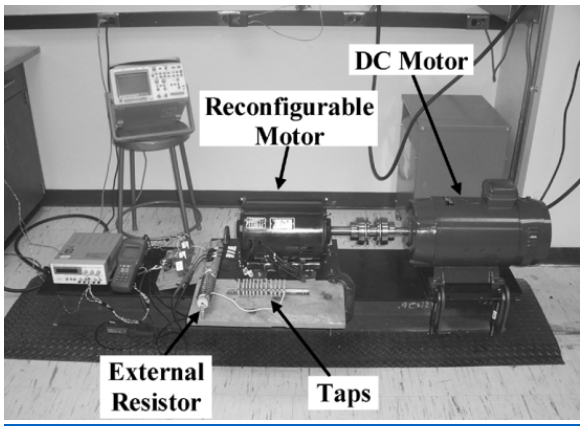


**Fig. 2.** Experimental setup.

This paper consists of three other sections. The first section is on the design concept and methodology of construction of the reconfigurable induction motor. The second section presents the experimental setup (see Fig. 2) and test results obtained under normal operation using both the cast-type and reconfigurable squirrel cages. This section also contains results of faulty operations for stator winding faults. In the same section, certain fault diagnostic techniques such as the pendulous oscillation phenomenon [7]–[8][9] and the negative sequence component concept [1]–[2][3] were utilized to diagnose the stator winding interturn faults using the experimentally acquired motor fault signature data. The purpose of such tasks is to verify the performance of the reconfigurable induction motor under healthy and faulty conditions. In addition, this section includes the rotor broken bar faults under load conditions and the diagnostic results using the FFT [4], [5] and the pendulous oscillation [7]–[8][9] techniques, as well as the associated analysis of the reconfigurable squirrel-cage drawback issues. Finally, conclusions and recommendations are presented in the final section.

## SECTION II. Reconfigurable Motor Design Concept and Methodology

The design of the reconfigurable motor was accomplished with the help of the frame size and configuration of an existing induction motor rated at 5-hp. In other words, the motor housing and the stator core of this existing 5 hp induction motor were used as the base design for the new reconfigurable induction motor. The remainder of the design consists of the rotor core, the rotor cage including the rotor bars and the end rings, the shaft, the end cap that is used to secure the rotor bars into the end rings, and the stator winding connections including winding taps to enable one to emulate a wide variety of stator short-circuit faults. The detailed design concepts of these reconfigurable motor components are given in the following sections.

### A. Stator Design

As mentioned earlier, the stator core was fabricated in such a manner so as to be identical to that of an existing 5-hp induction motor. The stator core consists of 36 slots, i.e., in this machine, there are six slots per pole (for a six-pole motor) and two slots per pole per phase. A cross-sectional view of the motor is depicted in Fig. 3. To minimize the inherent cogging torque effects due to the space harmonics arising from the magnetic circuit geometric configurations and the effects of winding layouts, the stator core was skewed by one slot pitch, i.e., by $30^{\circ}e$. The skewed stator including its winding coils is shown in Fig. 4. Meanwhile, the stator phase windings are double layered, lap connected with short-pitched coils, each with a span of $150^{\circ}e$ (see Fig. 5). The reason for skewing the stator and not skewing the rotor was to facilitate/ease the dismantling of the rotor cage bars when necessary for rotor fault emulation purposes.

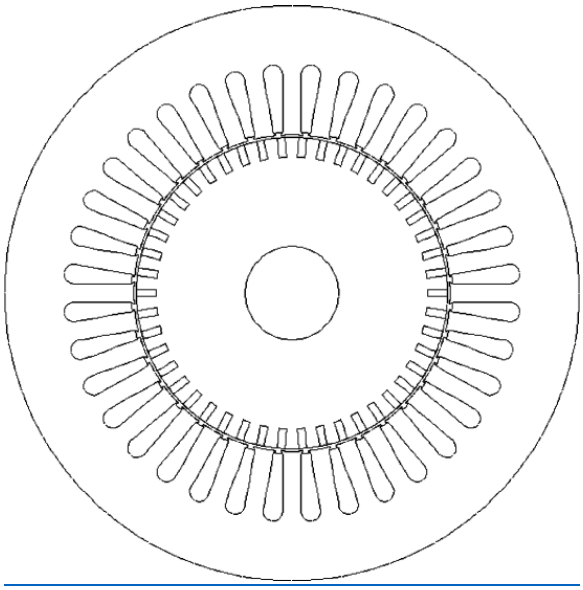

**Fig. 3.** Cross-sectional view of 5-hp reconfigurable motor.

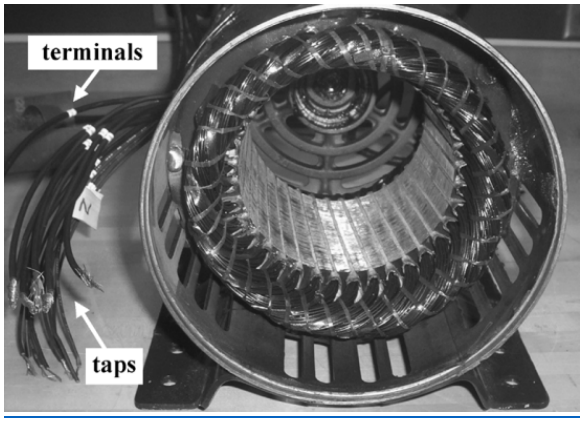


**Fig. 4.** Skewed stator with winding coils and taps.

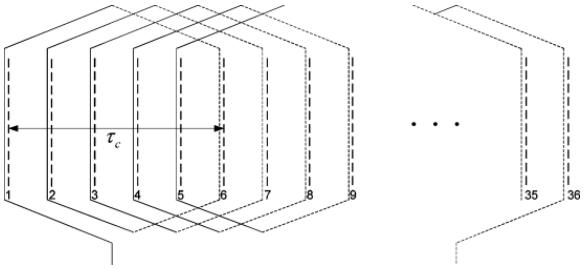


**Fig. 5.** Stator winding layouts with short-pitched coils.

In order to emulate stator interturn short-circuit faults, the motor had a phase winding that was prepared with taps for purposes of “experimental mimicking” of incipient interturn faults. Here, incipient stator faults have been emulated by varying the resistance between the taps, and consequently, varying the magnitude of the circulating fault current. Hence, in this approach, physical mechanisms of insulation failure are not emulated but rather the effects of partial insulation failure prior to a complete insulation breakdown are considered. In this approach, the condition of the stator winding insulation is evaluated based on the magnitude of the circulating fault current only in the very early stages of insulation weakening. No attempt at the study of the progression of insulation failure was intended here. Ten taps were soldered sequentially every two turns, beginning with the “start” point of turn #1 and ending with the “start” point of turn #19 in only one phase of the machine (see the

schematic winding diagram of Fig. 6). The limited number of taps to be soldered in the windings is restricted by the amount of space available inside the motor housing. These taps are specially added at the motor terminal of one of the phases since the stator faults are likely to occur closest to the terminal end of the windings due to insulation stresses caused by the high switching effects from pulsewidth-modulated (PWM) drives [18]. To limit the short-circuit loop current, a variable external resistor was connected between the taps of the shorted portion of the winding turns (see Fig. 6). The design characteristics of this reconfigurable induction motor are given in Table II.

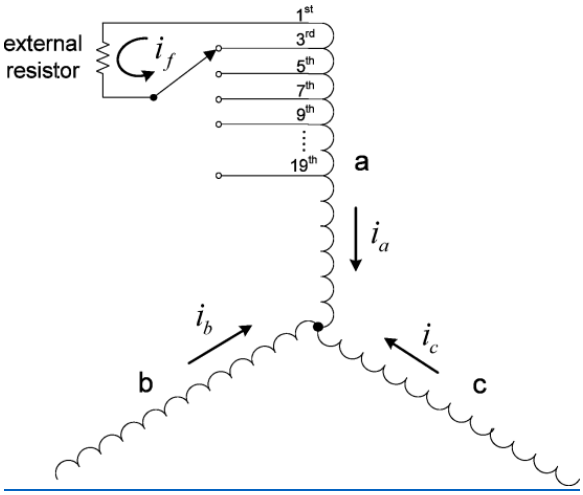


**Fig. 6.** Schematic diagram of stator windings with taps.

**Table II** 5-HP Induction Motor Characteristics

| | |
|---|---|
| Power (hp) | 5 |
| Voltage (V) | 230/460 |
| Current (A) | 16.2/8.1 |
| Speed (r/min) | 1150 |
| Number of Poles | 6 |
| Number of Coils Per Phase | 12 |
| Number of Turns Per Coil | 20 |
| Number of Turns Per Phase | 240 |
| Type of Stator Windings | Double-Layer, Lap |
| Number of Stator Slots | 36 |
| Number of Rotor Bars | 46 |
| Number of Taps (in phase a) | 10 |

## B. Rotor Design

A production-type aluminum die-cast squirrel-cage, see Fig. 7, was prototyped for use with this motor to help collect a baseline healthy performance experimental database. Previous efforts for emulating broken rotor bar faults have required different rotor bars to be broken by drilling out portions of such bars to physically break the continuity of the current conduction path through such bars. This process of emulating broken bar faults requires custom machining, and the action (damage) performed on such rotors is irreversible. This method of bar breaking essentially limits the mix of combination and number of broken bars that can practically be made available for testing in a given motor, such as varying combinations of adjacent or nonadjacent bar breakages, which would necessitate a separate rotor for each desired set of broken bar configuration or scenario. A broken bar fault generally implies the presence of a nonconductive discontinuity (air gap) between the two broken bar

sections. Therefore, this leads to the idea of constructing a reconfigurable rotor in which the rotor bars can be removed at will to emulate broken bar faults. The thinking was that the advantage of this reconfigurable rotor lies in its ability to create a large number of combinations of broken bar fault scenarios using the same rotor cage and the potential reversibility of such bar breakages.

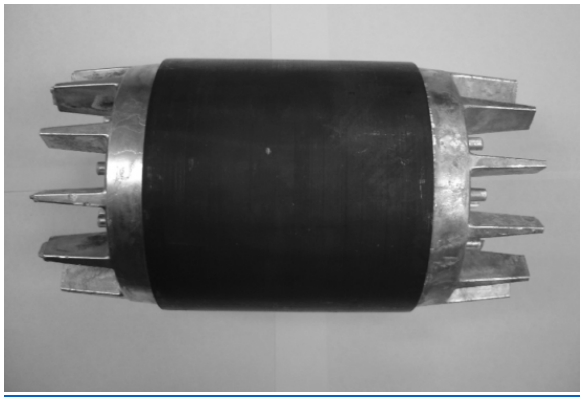

**Fig. 7.** Die-cast squirrel-cage rotor.

The core was manufactured from the same type of steel laminations that were used to manufacture the stator core. As mentioned before, for the convenience of inserting the rotor bars into the lamination stack, the rotor core was not skewed. Again, in order to eliminate any cogging effect present in the motor torque due to space harmonic effects, the stator core, as mentioned before, was skewed by one stator slot pitch of $30^{\circ}e$. Since the rotor core was not skewed, the rotor bars were accordingly designed to have a layout parallel to the axis of rotation, and they were fabricated from a copper alloy (see Figs. 8 and 9). The rotor end rings were also made of the same material as the rotor bars, and the geometry of the end rings were designed with an outer diameter equal to that of the rotor core. The design was conceived in such a manner that it allows the end rings to be removed, and hence, the rotor bars become easily accessible for removal or insertion from or into the rotor slots. Due to the fact that the rotor bars are not welded to the end rings, such as in typical motor designs, the slots of the end rings were generously coated with conductive grease to ensure a good electrical conduction path to the bars. The rotor bars and the end rings as well as the complete rotor are depicted in Figs. 8 and 9, respectively. In this reconfigurable motor, there are a total of 46 rotor bars.

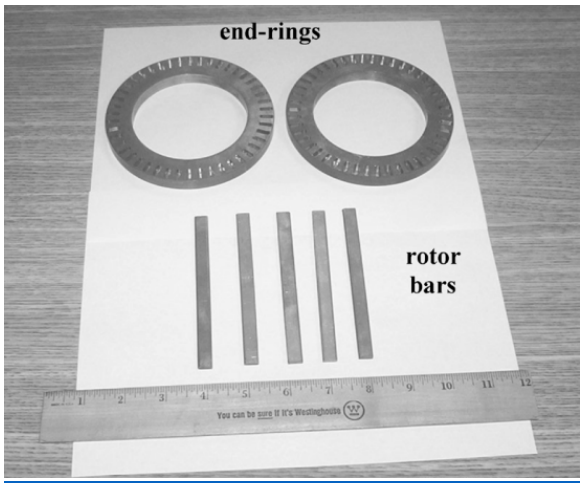


**Fig. 8.** Rotor bars and end rings.

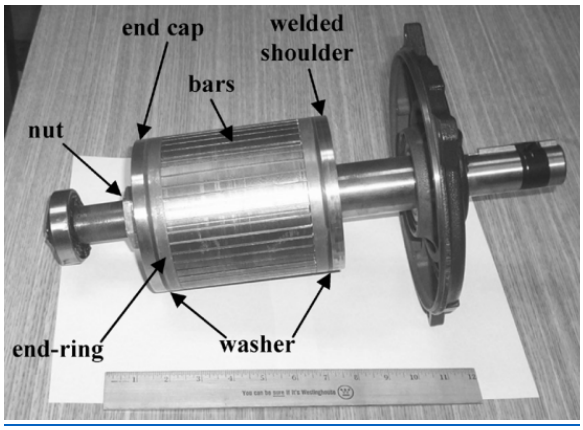


**Fig. 9.** Reconfigurable squirrel-cage rotor.

## C. Shaft and End Cap Design

The shaft was constructed by machining a steel rod to its desired geometry. Two keyways, which were 180˚*e* from each other, were milled into the shaft to secure the rotor core. In a typical production induction motor of this size and rating, the rotor core, including the aluminum die-cast cage, is “hot dropped” on the shaft to form one inseparable assembly. This is not the case for the reconfigurable rotor at hand. Here, a custom shoulder was welded to the drive end of the shaft in order to secure the position of one of the end rings. A nonconductive washer was added to act as an insulator between the shoulder and the end ring (see Fig. 9). Meanwhile, opposite to the drive end of the shaft, in order to tighten the other end ring to the rotor core, an end cap of the same diameter as the rotor was designed to slide down the shaft to secure that end ring. Again, a nonconductive washer was added as an insulator between the end cap and that end ring (see Fig. 9). Threads were added to the nondrive end of the shaft so that the end cap could be secured to the end ring using a nut (see Fig. 9 for the details). Meanwhile, a keyway was inserted in the square slot formed by the rotor and the end cap to secure these parts to the shaft so that they rotate as one piece with the shaft.

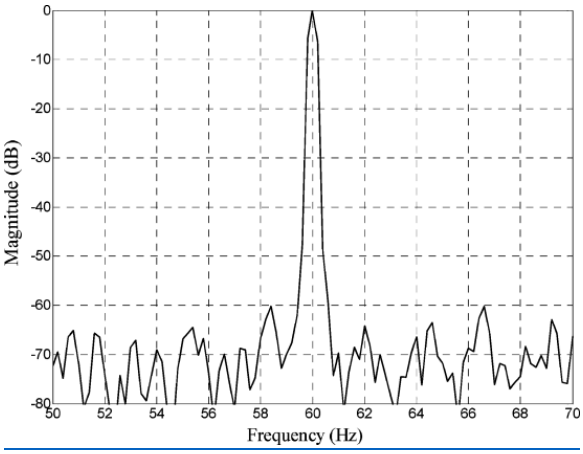


**Fig. 10.** Phase current FFT of healthy die-cast rotor cage.

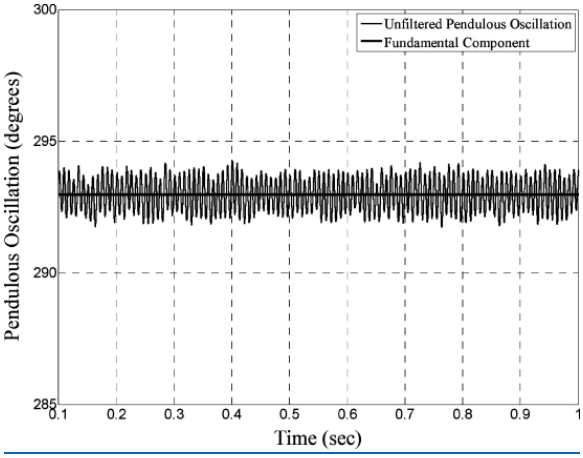


**Fig. 11.** Healthy die-cast rotor cage pendulous oscillation.

# SECTION III. Experimental Results and Analysis

## A. Healthy Motor Test Results

The motor was tested at full load and rated frequency using the die-cast squirrel-cage rotor. It should be mentioned that the motor was energized from an open loop (constant volts per hertz) commercially available PWM-inverter drive. The resulting FFT spectrum of its stator current waveform is given in Fig. 10. Its corresponding profile of the magnetic field pendulous oscillation, which is the time-domain profile of the angle between the current and voltage space vectors at the motor terminals, [7]–[8][9] is given in Fig. 11. For completeness and convenience of the reader, the magnetic field pendulous oscillation angle $\delta(t)$ associated with broken rotor bars or rotor conduction defects is a function of time, and is the instantaneous phase angle difference between the motor's stator voltage space vector $v_s^{\rightharpoonup}$ and the stator current space vector $i_s^{\$rightharpoonup\$}$. Accordingly, $\delta(t) = \angle v_s^{\rightharpoonup} - \angle i_s^{\$rightharpoonup\$}$, while the so-called swing angle $\Delta\delta_1 = \delta_{\max} - \delta_{\min}$ is the peak-to-peak magnitude of the fundamental component of the pendulous oscillation angle $\delta(t)$ of frequency $(2sf)$, where s is the slip and $f$ is the supply frequency. For further details on this diagnostic method, [7]–[8][9] should be consulted. The lack of presence of any distinct lower sideband (LSB) in the FFT spectrum of Fig. 10 indicates that there are no broken bars or anomalies such as interbar lamination shorts presence in this cage. The lack of a fundamental $(2sf)$ component of pendulous oscillation angle in Fig. 11 confirms the lack of bar breakage or other squirrel-cage anomalies in this die-cast baseline case.

## B. Test Results of Stator Interturn Shorts

Test data were collected on stator winding interturn shorts using the reconfigurable rotor for this case of the subject 230/460-V, six-pole, 5-hp, squirrel-cage induction motor fed from a commercially available PWM-inverter drive. The test was performed under open-loop (constant volts per hertz) PWM control excitation fed from a 460-V utility supply. The stator interturn fault test data presented herein were obtained under healthy, 2, 6, 10, 12, 14, and 16 shorted turns (STs) at 50% load condition. The interturn short circuit was achieved through an external resistor of 1 Ω, see Fig. 6, in order to restrict the shorted loop current $I_f$ to a safe level of current that does not cause permanent coil damage.

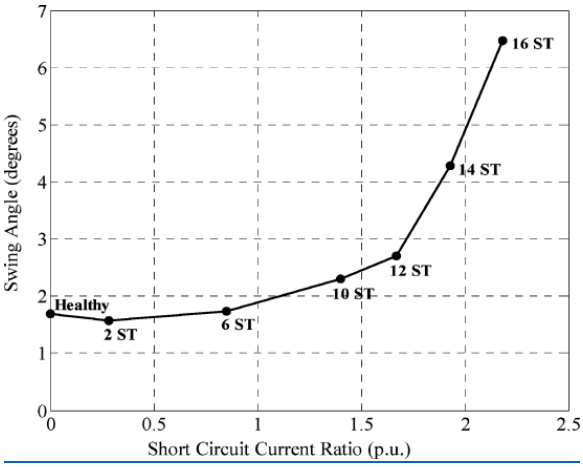


**Fig. 12.** Swing angle $\Delta\delta_1$ versus the short-circuit current ratio $I_f/I_p$.

In order to verify the motor performance under interturn short-circuit fault conditions, two fault diagnostic techniques, namely the pendulous oscillation phenomenon [7]–[8][9] and the negative sequence component concept [1]–[2][3], were utilized. As reported in [9], the range of the pendulous oscillation (swing angle) progressively increases with an increase in the number of STs, provided that the amplitude of the circulating loop (fault) current $I_f$ exceeds the amplitude of the line current $I_a$ (or the positive sequence component of stator currents $I_p$). This progressive increase in the swing angle magnitude $\Delta\delta_1$ with the number of STs can be observed in Fig. 12 and Table III. Note that in Fig. 12, the swing angle $\Delta\delta_1$ is plotted with respect to the circulating loop current ratio $I_f/I_a$ (or $I_f/I_p$). A similar trend can also be observed using the negative sequence component concept [1]–[2][3] as illustrated in Fig. 13 and Table III. Note that in Fig. 13, the magnitude of the negative sequence component of stator currents In progressively increases with an increase in the number of STs, if and only if the circulating loop current exceeds the line current. It is of importance to mention that the swing angle and the negative sequence current component are nonzero under a healthy condition due to the inherent motor manufacturing imperfections that resulted in slight unbalances in the motor phase $a$, $b$, and $c$ currents. From these test results, one can conclude that the reconfigurable motor has the capability of emulating stator winding interturn faults.

**Table III** 5-HP Reconfigurable Motor Diagnostic Results

| ST | $\Delta\delta°$ | $I_n(A)$ | $I_p(A)$ | $I_f(A)$ |
|---|---|---|---|---|
| **0** | 1.689 | 0.107 | 9.011 | 0.000 |
| **2** | 1.574 | 0.091 | 8.996 | 2.566 |
| **6** | 1.732 | 0.108 | 9.040 | 7.697 |
| **10** | 2.302 | 0.147 | 9.157 | 12.829 |
| **12** | 2.703 | 0.173 | 9.225 | 15.394 |
| **14** | 4.286 | 0.298 | 9.298 | 17.960 |
| **16** | 6.478 | 0.443 | 9.411 | 20.526 |

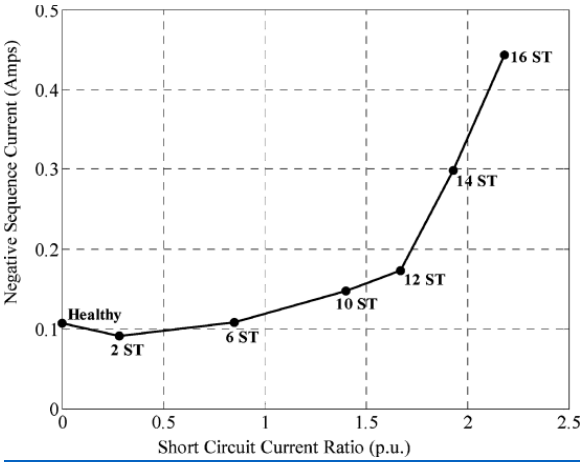


**Fig. 13.** Negative sequence current In versus the short-circuit current ratio $I_f/I_p$.

## C. Test Results of Reconfigurable Rotor Faults

In the reconfigurable squirrel-cage case, the rotor circuit did not yield consistent results when operated under healthy condition, i.e., with none of the rotor bars missing. The spectrum of the phase currents corresponding to this healthy case shows considerable LSB and upper sideband (USB) (see Fig. 14), thus indicating the presence of poor electrical contacts between the end rings of the cage and one or more of the removable bars. This is despite the presence of the conducting film of coating between these bars and the end rings.

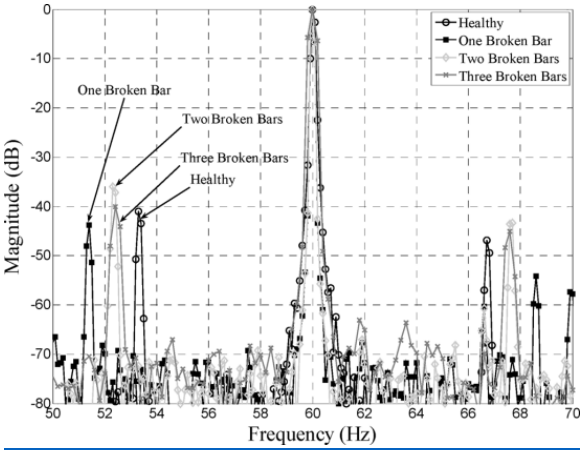


**Fig. 14.** Phase current FFT of healthy, one broken bar, two broken bars, and three broken bars.

Furthermore, a test was conducted involving electrically insulating one of the end rings at the nondrive end of the rotor, with the motor being energized for starting purposes. Normally, one would expect zero starting torque, and hence, no rotation. However, it was observed that the motor exhibited a nonzero starting torque and the shaft began to turn as a result. This indicated to these investigators the presence of current loops in the cage that could have only resulted from circuit shorts between the rotor laminations and some of the bars, i.e., the presence of the so-called interbar lamination shorts. This may be the result of damage to the lamination insulation due to the repeated assembly and disassembly process performed on this reconfigurable cage during the course of performing all these tests. Such shorts lead to asymmetry in the rotor MMF waveforms and to the existence of a forward rotating component of MMF at $(sf)$ frequency and a backward rotating component at $(-sf)$ frequency with respect to the rotor that is rotating forward at a frequency $(1-s)f$. The latter $(-sf)$ component gives rise to the $(1-2s)f$ component of current in the stator that is seen in the current FFT spectrum as LSB under a condition with all bars present in this rotor. As mentioned before, this is in addition to the possible presence of bad conductive contacts between the bars and the end rings resulting from the

repeated disassembly and assembly process. Thus, this leads to the appearance of conductive discontinuities in the rotor loop currents and the appearance of effects that resemble the presence of broken bars. Again, the use of conductive grease at the bar contact tips with the end rings did not considerably improve the performance of the motor. In summary, after numerous attempts to mechanically make sure that good contact between the bar ends and the end ring do exist, the problem of conductive discontinuities persisted. This leads the authors to conclude that the present design of the reconfigurable rotor leaves much to be desired. Thus, such a design is not recommended for use and implementation by future investigators in this area.

The FFT spectra of the motor phase currents corresponding to different fault scenarios were obtained by the removal of one, two, or three bars from the reconfigurable cage. These FFT spectra are depicted in Fig. 14. The fact that the sideband components did not follow the expected pattern of an increase in their magnitude with a corresponding increase in the number of bars removed from the cage can be attributed to the fact that the quality of the surface contact resistances between the end rings and the bars could not be guaranteed in their consistency. Therefore, these contact resistances change from case to case because of the required disassembly of the rotor cage between the conduction of the various tests in the laboratory. Upon close examination of the location of the LSB frequencies $(1-2s)f$ in Fig. 14, for one, two, and three removed bar tests, emulating one, two, and three bar breakages, it is found that the values of the specific LSB frequencies for each of these cases are different from one another. This can be explained as given next. Since these tests were all conducted at rated developed torque of 30 Nm (full-load condition), and since this torque is proportional to $R_2/s$, where $R_2$ is the equivalent rotor resistance reflected into the stator side and $R_2$ varies in value for each of the cases of one, two, and three removed bars, it follows that the running slip s, which yields the 30 Nm torque will have distinct and separate values for each of these cases. Hence, the LSB frequency $(1-2s)\,f$ will be different for each of the aforementioned "broken-bar" scenarios. These distinct and different LSB frequencies are clearly apparent in the stator current test FFT spectral results of Fig. 14.

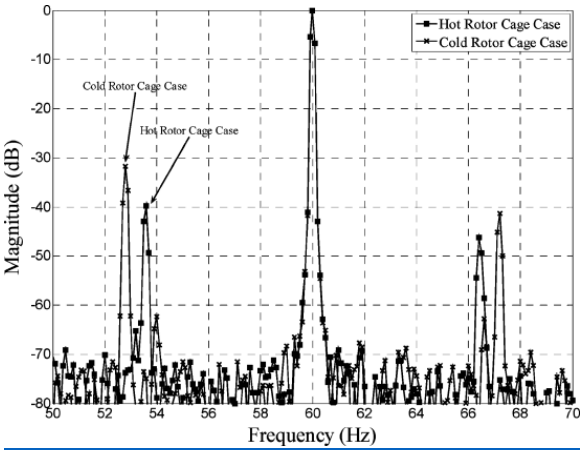


**Fig. 15.** Healthy rotor cage phase current FFT showing temperature dependence.

Meanwhile, it was also found that the sideband components are highly dependent on the rotor cage temperature, as illustrated for rotor cold and hot conditions in Fig. 15 (under healthy case with no broken/removed bars). This FFT spectrum of Fig. 15 again tends to allude to the uneven distribution of contact pressure and resistances between the rotor bars and the end rings. It should be observed that, for the same 30 Nm torque, the $R_2/s$ ratio should remain the same for cold and hot rotor conditions. Despite the rise in rotor temperature, which at first glace would lead one to think may lead to a rise in $R_2$, the opposite seems to have happened here. This is because under hot condition, the value of $R_2$ appears to be lower due to higher contact pressure caused by bar metal expansion inside the bar holes in the end ring under heat. It follows that the corresponding running slip will be lower in value under hot conditions than in cold conditions to keep

the $R_2/s$ ratio constant. This is born out by the location of LSB frequencies in the FFT of the stator current spectra shown in Fig. 15 for these two conditions.

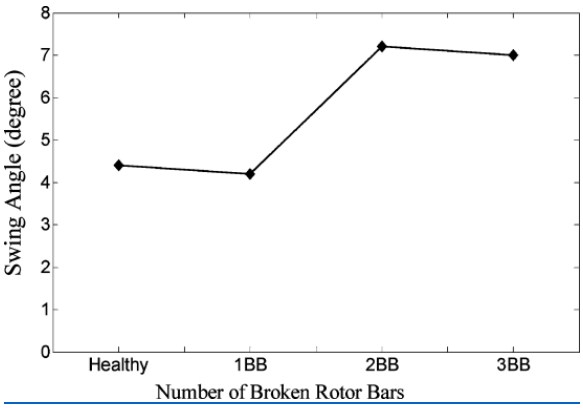


**Fig. 16.** Swing angle $\Delta\delta_1$ of healthy, one broken bar, two broken bars, and three broken bars.

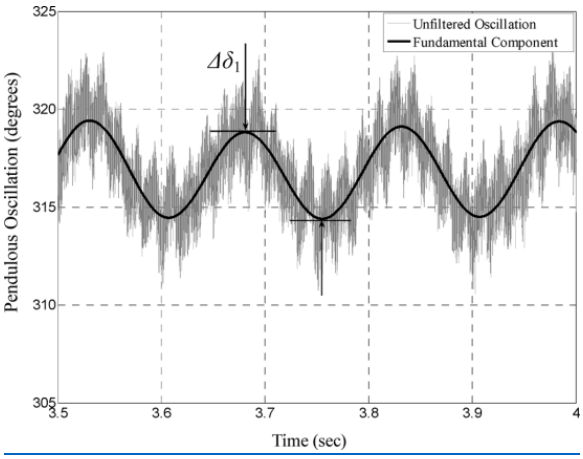


**Fig. 17.** Healthy rotor cage pendulous oscillation. Swing angle $\Delta\delta_1 = 4.4^{\circ}$.

The stator current test data for the healthy, one, two, and three removed bar (broken-bar) tests in conjunction with the corresponding motor terminal voltage test data were reexamined using the pendulous oscillation method [7]–[8][9]. Again, in this method [7]–[8][9], the time-domain profile of the angle between the stator current space vector, and the stator voltage space vector renders the so-called swing angle $\Delta\delta_1$, which constitutes the variable leading to the "broken-bar" fault index. Normally, under healthy rotor condition, $\Delta\delta_1$ is expected to be negligible. These swing angle findings are given for the healthy and one through three removed/broken bars in Fig. 16. Depicted in Fig. 17 is the time-domain profile of the pendulous oscillation angle for the healthy rotor cage case. It is expected that the peak-to-peak value of the pendulous oscillation known, namely, as the swing-angle $\Delta\delta_1$ in the healthy case should be negligible as shown earlier for the

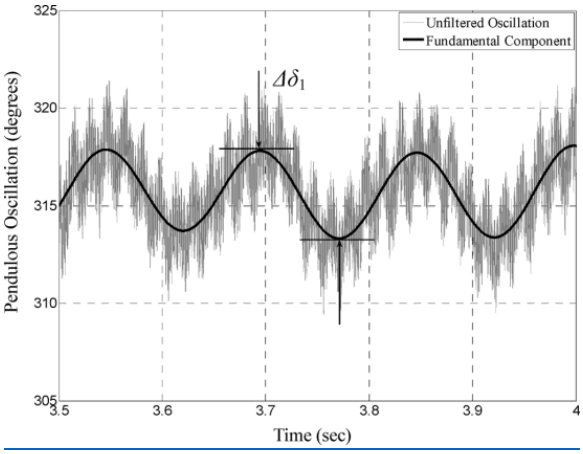


**Fig. 18.** One broken bar pendulous oscillation. Swing angle $\Delta\delta_1 = 4.2^{\circ}$.

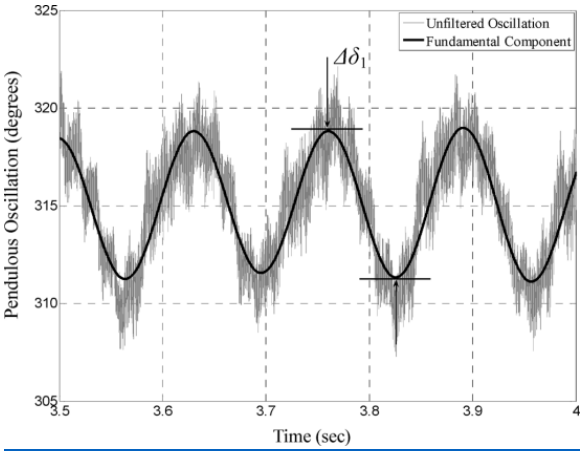


**Fig. 19.** Two broken bars pendulous oscillation. Swing angle $\Delta\delta_1 = 7.2^{\circ}$.

die-cast cage of Fig. 11. However, as can be seen from Fig. 17, this is not the case for this reconfigurable cage, meaning that there is a considerable distortion of the rotor magnetic field even in the healthy rotor cage case. This can only result from conductive discontinuities in the cage circuit "masquerading" as bar breakages. Depicted in Figs. 18–20 are the time-domain profiles of the pendulous oscillation angle for the cases with one, two, and three removed/broken bars under full-load 30 Nm operating conditions. Normally, one would have observed larger magnitudes of the pendulous oscillations as the number of removed bars increased from one to two to three. However, the expected monotonic trend demonstrated earlier in [7]–[8][9] did not hold here. This indicates problems with the contact resistances between bars and end rings, each time the rotor is disassembled and reassembled between the processes of removal of the bars and conducting the tests. Therefore, as can be seen from the earlier results, both diagnostic techniques used before are in close agreement in so far as demonstrating the present inadequacies of the reconfigurable rotor for broken bar fault emulation purposes. Therefore, in summary, these authors recommend that future investigators should not replicate the present rotor design for purposes of broken bar emulation. Hence, they consider that one of the contributions of this paper is to warn investigators about the difficulties that arose with the present design despite the mitigation measures that have been attempted in their effort to make this concept a success. The present rotor design concept cannot be considered a success in light of the results presented here.

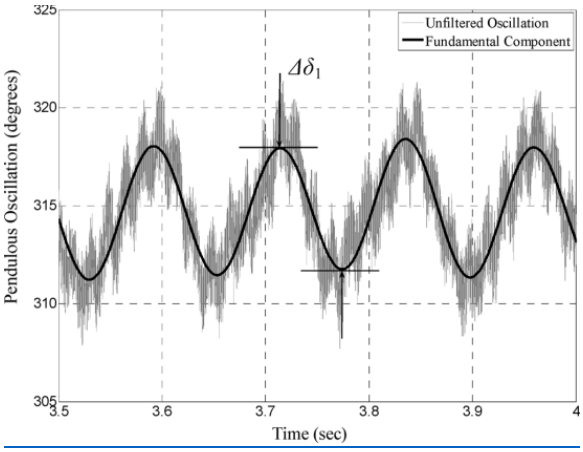


**Fig. 20.** Three broken bars pendulous oscillation. Swing angle $\Delta\delta_1 = 7^\circ$.

## SECTION IV. Conclusion and Recommendations

A 5-hp reconfigurable induction motor, which was designed for emulation of stator winding interturn and broken rotor bar faults, has been introduced. The experimental results obtained under stator interturn faults have demonstrated that the reconfigurable motor has successfully emulated stator interturn faults, which is further verified through the use of two diagnostic methods, namely the pendulous oscillation phenomenon and the negative sequence component concept. A complete set of test results, including a healthy rotor core using a die-cast rotor and rotor broken bar fault emulations using the reconfigurable rotor has been presented. It was found based on the current spectrum sideband analysis and magnetic field pendulous oscillation swing angle analysis that the electrical surface contacts between bars and end rings in the reconfigurable cage and electrical shorts between bars and lamination material presented a problem that leads to the appearance of bar breakage indication where no such bar breakages are present. Hence, these authors are led to recommend that the present reconfigurable rotor design concept for bar fault emulation cannot be considered a success. However, a major effort has to be done toward improving the quality and uniformity of contact resistances between the rotor bars and end rings, such as using a bolted connection between the rotor bars and end rings.

## ACKNOWLEDGMENT

The authors would like to acknowledge the support of the A.O. Smith Corporation, which supplied and guided the manufacturing of the motor components. They further acknowledge ideas suggested by the reviewers that were incorporated into this paper.

## References

**1.** G. B. Kliman, W. J. Premerlani, R. A. Koegl and D. Hoeweler, "A new approach to on-line turn fault detection in ac motors", *Proc. IEEE Ind. Appl. Conf. Annu. Meet.*, vol. 1, pp. 687-693, 1996.

**2.** J. L. Kohler, J. Sottile and F. C. Trutt, "Alternatives for assessing the electrical integrity of induction motors", *IEEE Trans. Ind. Appl.*, vol. 28, no. 5, pp. 1109-1117, Sep./Oct. 1992.

**3.** R. M. Tallam, T. G. Habetler and R. G. Harley, "Stator winding turn-fault detection for closed-loop induction motor drives", *IEEE Trans. Ind. Appl.*, vol. 39, no. 3, pp. 720-724, May/Jun. 2003.

**4.** A. Bellini, F. Filippetti, G. Franceschini, C. Tassoni and G. B. Kliman, "Quantitative evaluation of induction motor broken bars by means of electrical signature analysis", *IEEE Trans. Ind. Appl.*, vol. 37, no. 5, pp. 1248-1255, Sep./Oct. 2001.

**5.** N. M. Elkasabgy, A. R. Eastham and G. E. Dawson, "Detection of broken bars in the cage rotor of an induction machine", *IEEE Trans. Ind. Appl.*, vol. 28, no. 1, pp. 165-171, Jan./Feb. 1992.

**6.** H. A. Toliyat and T. A. Lipo, "Transient analysis of cage induction machines under stator rotor bar and end ring faults", *IEEE Trans. Energy Convers.*, vol. 10, no. 2, pp. 241-247, Jun. 1995.
**7.** B. Mirafzal and N. A. O. Demerdash, "Induction machine broken-bar fault diagnosis using the rotor magnetic field space-vector orientation", *IEEE Trans. Ind. Appl.*, vol. 40, no. 2, pp. 534-542, Mar./Apr. 2004.
**8.** B. Mirafzal and N. A. O. Demerdash, "Effects of load magnitude on diagnosing broken bar faults in induction motors using the pendulous oscillation of the rotor magnetic field orientation", *IEEE Trans. Ind. Appl.*, vol. 41, no. 3, pp. 771-783, May/Jun. 2005.
**9.** B. Mirafzal and N. A. O. Demerdash, "On innovation methods of induction motor interturn and broken-bar fault diagnostics", *IEEE Trans. Ind. Appl.*, vol. 42, no. 2, pp. 405-414, Mar./Apr. 2006.
**10.** C.-C. Yeh, B. Mirafzal, R. J. Povinelli and N. A. O. Demerdash, "A condition monitoring vector database approach for broken bar fault diagnostics of induction machines", *Proc. IEEE Int. Electr. Mach. Drives Conf.*, vol. 1, pp. 29-34, 2005.
**11.** G. B. Kliman, R. A. Koegl, J. Stein, R. D. Endicott and M. W. Madden, "Noninvasive detection of broken rotor bars in operating induction machines", *IEEE Trans. Energy Convers.*, vol. 3, no. 4, pp. 873-879, Dec. 1988.
**12.** M. E. H. Benbouzid, "Bibliography on induction motors faults detection and diagnosis", *IEEE Trans. Energy Convers.*, vol. 14, no. 4, pp. 1065-1074, Dec. 1999.
**13.** A. Stavrou, H. G. Sedding and J. Penman, "Current monitoring for detecting interturn short circuits in induction motors", *IEEE Trans. Energy Convers.*, vol. 16, no. 1, pp. 32-37, Mar. 2001.
**14.** M. E. H. Benbouzid and G. B. Kliman, "What stator current processing-based technique to use for induction motor rotor faults diagnosis?", *IEEE Trans. Energy Convers.*, vol. 18, no. 2, pp. 238-244, Jun. 2003.
**15.** "Report of large motor reliability survey of industrial and commercial installation Part I and Part II", *IEEE Trans. Ind. Appl.*, vol. 21, no. 4, pp. 853-872, Jul./Aug. 1985.
**16.** P. F. Albrecht, J. C. Appiarius and D. K. Sharma, "Assessment of the reliability of motors in utility applications—Updated", *IEEE Trans. Energy Convers.*, vol. 1, no. 1, pp. 39-46, Dec. 1986.
**17.** J. F. Bangura and N. A. O. Demerdash, "Diagnosis and characterization of effects of broken rotor bars and connectors in squirrel-cage induction motors by a time-stepping coupled finite element-state space modeling approach", *IEEE Trans. Energy Convers.*, vol. 14, no. 4, pp. 1167-1176, Dec. 1999.
**18.** N. A. O. Demerdash, Electrical Transients and Surges in Power Systems and Devices, WI, Milwaukee:Marquette Univ. (Class Notes), 2005.